Polymer 51 (2010) 5058–5070

Contents lists available at ScienceDirect

Polymer

journal homepage: www.elsevier.com/locate/polymer

Novel acrylic nanocomposites containing in-situ formed calcium phosphate/layered silicate hybrid nanoparticles for photochemical rapid prototyping, rapid tooling and rapid manufacturing processes

Matthias Gurr [a,b], Yi Thomann [a], Michael Nedelcu [a], Rainer Kübler [b], Laszlo Könczöl [b], Rolf Mülhaupt [a,c,*]

[a] Institut für Makromolekulare Chemie und Freiburger Materialforschungszentrum der Albert-Ludwigs-Universität, Stefan-Meier-Straße 21/31, D-79104 Freiburg i. Br., Germany
[b] Fraunhofer-Institut für Werkstoffmechanik IWM, Wöhlerstraße 11, D-79108 Freiburg i. Br., Germany
[c] Freiburg Institute for Advanced Studies, School of Soft Matter Research, Albertstraße 19, D-79104 Freiburg i. Br., Germany

ARTICLE INFO

Article history:
Received 12 June 2010
Received in revised form
18 July 2010
Accepted 12 August 2010
Available online 20 August 2010

Keywords:
Rapid prototyping
Nanocomposites
Stereolithography

ABSTRACT

Novel acrylic nanocomposites containing calcium phosphate/layered silicate hybrid nanoparticles have been developed for use in photochemical Rapid Prototyping processes like Structural Light Modulation (SLM) and Stereolithography (SL). When tertiary alkyl amines, protonated with phosphoric acid, were added to an acrylic suspension of calcium bentonite, the cation exchange of Ca^{2+} rendered bentonite organophilic, caused swelling, intercalation and dispersion of silicate nanoplatelets in the monomer. The simultaneous precipitation of calcium phosphate onto the silicate nanoplatelets accounted for the in-situ formation of hybrid nanoparticles. The uniform dispersions of such hybrid nanoparticles afforded a high degree of shear thinning, reflecting the presence of anisotropic filler particles, and increased photosensitivity in SLM with respect to the unfilled resin. Young's modulus of green and postcured parts increased by 30% at a filler content of 15 wt.% with respect to that of the unfilled benchmark material. This enhanced stiffness was paralleled by 30% increased fracture toughness. As evidenced by fracture surface analysis using Environmental Electron Microscopy (ESEM) and optical microscopy, the improved energy dissipation at the crack tip correlated with roughness of the fracture surfaces, increasing with increasing filler content. Moreover, the examination of the volumetric polymerization shrinkage and the fabrication of H-shaped diagnostic specimens revealed that the nanocomposites were processed with high accuracy, increasing with increasing filler content. Nanocomposite morphologies, examined by means of Transmission Electron Microscopy (TEM), demonstrated that the large primary bentonite particles with average diameters >10 μm fragmented into much smaller particles with average diameters in the range of 1 μm. According to TEM and Wide Angle X-Ray Scattering (WAXS), such in-situ formed nanoparticles were composed of both stacks of organoclay nanoplatelets and also isolated nanoplatelets typical for fully exfoliated organoclays.

1. Introduction

Layered Manufacturing (LM) technology has made significant progress during the last decade [1]. With improving accuracy, time and cost efficiency have improved and the scope of application has widened considerably. Additive and freeform layerwise fabrication of 3D models today is not limited to visualizing designs of prototypes in Rapid Prototyping (RP) anymore, but is applied for the preparation of functional prototypes and for tooling (Rapid Tooling) [2]. In some areas of application, especially those that require production of parts fitted to individual demands, end use parts are already manufactured using RP technologies. On-going improvement of processes and material properties will expand LM technology toward Rapid Manufacturing (RM).

All LM technologies share the same virtual pre-processing. The model is either designed via CAD or obtained from 3D scanning or tomography, respectively. The respective model data is sliced into 2D layers that are sequentially generated physically in an RP apparatus. Layer formation and adhesion of adjacent layers is achieved following different physical and chemical principles in the variety of RP processes that were developed since Stereolithography (SLA) was brought to the market at first in 1986 [3]. Taking into account their individual strengths and specific

* Corresponding author. Institut für Makromolekulare Chemie und Freiburger Materialforschungszentrum der Albert Ludwigs-Universität Freiburg, Stefan-Meier-Straße 21/31, D-79104 Freiburg i. Br., Germany. Tel.: +49 761 203 6273; fax: +49 761 203 6319.
E-mail address: rolf.muelhaupt@makro.uni-freiburg.de (R. Mülhaupt).

0032-3861/$ – see front matter © 2010 Elsevier Ltd. All rights reserved.
doi:10.1016/j.polymer.2010.08.026

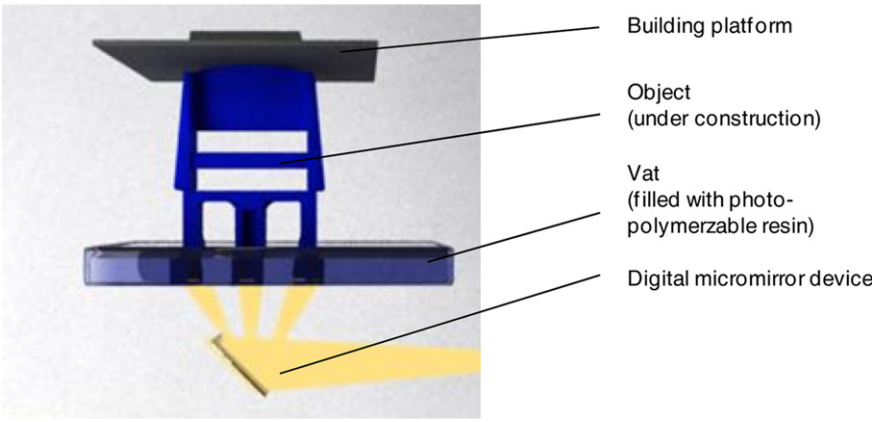

Scheme 1. Structural Light Modulation Process.

weaknesses, the user has to choose the technology which fits best the demands of specific applications [4]. In SLA and the related Structural Light Modulation process (SLM, Scheme 1), layer generation and adhesion is based on curing of a photosensitive resin. Curing is conducted either by scanning of the resin using a laser (SLA) or by curing the whole layer at once using a digital light processing system (SLM). Both techniques outperform other RP processes with respect to their high resolution in the range of 25–50 μm and their capability of realizing complex internal cavities and structures that cannot be built using other LM or subtractive freeform technologies [5].

In comparison to technologies working with functional materials like Fused Deposition Modelling (FDM) or Selective Laser Sintering (SLS), photochemical RP methods are limited regarding the choice of materials. The requirements set for resin viscosity and curing efficiency are commonly met using acrylic or epoxy resins that suffer from deficient mechanical properties, especially inherent brittleness that limits their application in RM [6,7]. Furthermore, polymerization shrinkage occurring during curing causes the development of internal stresses during the layer by layer building procedure. Their relaxation induces distortions and deviations from CAD data, thereby hindering possible applications in RT [8,9]. Various approaches have been reported on improvement in both the mechanical properties and building accuracy of materials for SLA and SLM. In the case of mechanical properties, these have mostly been focused on the improvement of polymer stiffness and strength. Increased stiffness has been obtained by incorporating continuous [10,11] or discontinuous glass fibres [10,12] and multiwalled carbon nanotubes [13,14], in all cases aligned with additional efforts in placing or dispersing the filler. Further composite materials containing either derivates of polyhedral oligomeric silsesquioxanes (POSS) [15], powdered silica [16] or surface modified silica nanoparticles [17–19] exhibit enhanced material stiffness. Material toughness has either not been characterized in the enumerated studies or was found not to be improved. Only very little research has been published concerning the incorporation of layered silicates into resins used for photochemical RP techniques [20]. These are well established as fillers in conventional thermosets, mostly based upon organoclays, and known to have potential for both toughening and stiffening of materials [21–24]. Preparation of organoclay dispersions is commonly conducted in a multistep procedure, beginning with the exchange of the intergallery ions for organic onium ions in aqueous medium followed by washing, drying, milling and redispersion of the filler in the respective matrix resin [25]. Additional requirements such as sedimentation stability over periods of weeks, sufficiently low viscosities and high curing efficiency have to be fulfilled in order to obtain improved and reproducible material properties in SLA or SLM processing. This paper reports the first systematic evaluation of organoclay dispersions as resins for photochemical RP techniques. A novel concept for the versatile and facile "one-pot" preparation of acrylic calcium phosphate/layered silicate hybrid nanoparticle dispersion was applied [26]. Clay functionalization, intercalation and dispersion were achieved in the acrylic monomer without requiring separate filler preparation and without the use of special dispersing agents. The influence of the hybrid nanoparticle content on the key properties of SLM and SLA resins has been analyzed, placing special emphasis upon the prospects of improving mechanical properties and building accuracy.

Table 1
Recipe for the formulation of unfilled matrix resin [17].

Description	Abbreviation	Acrylate functionality[a]	[wt.%]	M_n[a]
2,6-Di-*tert*-butyl-4-methylphenol (inhibitor)	BHT	–	1	220
Isocyanurate acrylate (oligomer)	G4302	3	11	2400
Modified aliphatic urethane acrylate (oligomer)	CN922	3	49	1300
Tris(2-hydroxyethyl) isocyanurate triacrylate (monomer)	SR368	3	15	423
Hexanediol diacrylate (reactive diluent)	HDDA	2	23	226

[a] According to product information.

2. Experimental part

2.1. Materials

Ca-bentonite EXM 918, which represents a natural montmorillonite with a cation exchange capacity (CEC) of 0.8 meq g^{-1}, was supplied by Süd-Chemie, Moosburg, Germany. The interlayer spacing calculated from wide angle X-ray scattering (WAXS) was 1.47 nm. Ethoquad C12 was supplied by Akzo-Nobel, Germany. Stearyl amine, hexanediol diacrylate and acryloyl chloride were purchased from Aldrich, Germany. Triethyl amine and methanol were purchased from Fluka, Germany. Phosphoric acid (85 %) and 2,6-di-*tert*-butyl-4-methylphenol (BHT) were purchased from Merck, Germany. 2-Hydroxyethyl methacrylate and methyl acrylate were purchased from Acros, Germany. Toluene was purchased from Roth, Germany. Acrylate functionalized oligomer CN922 and

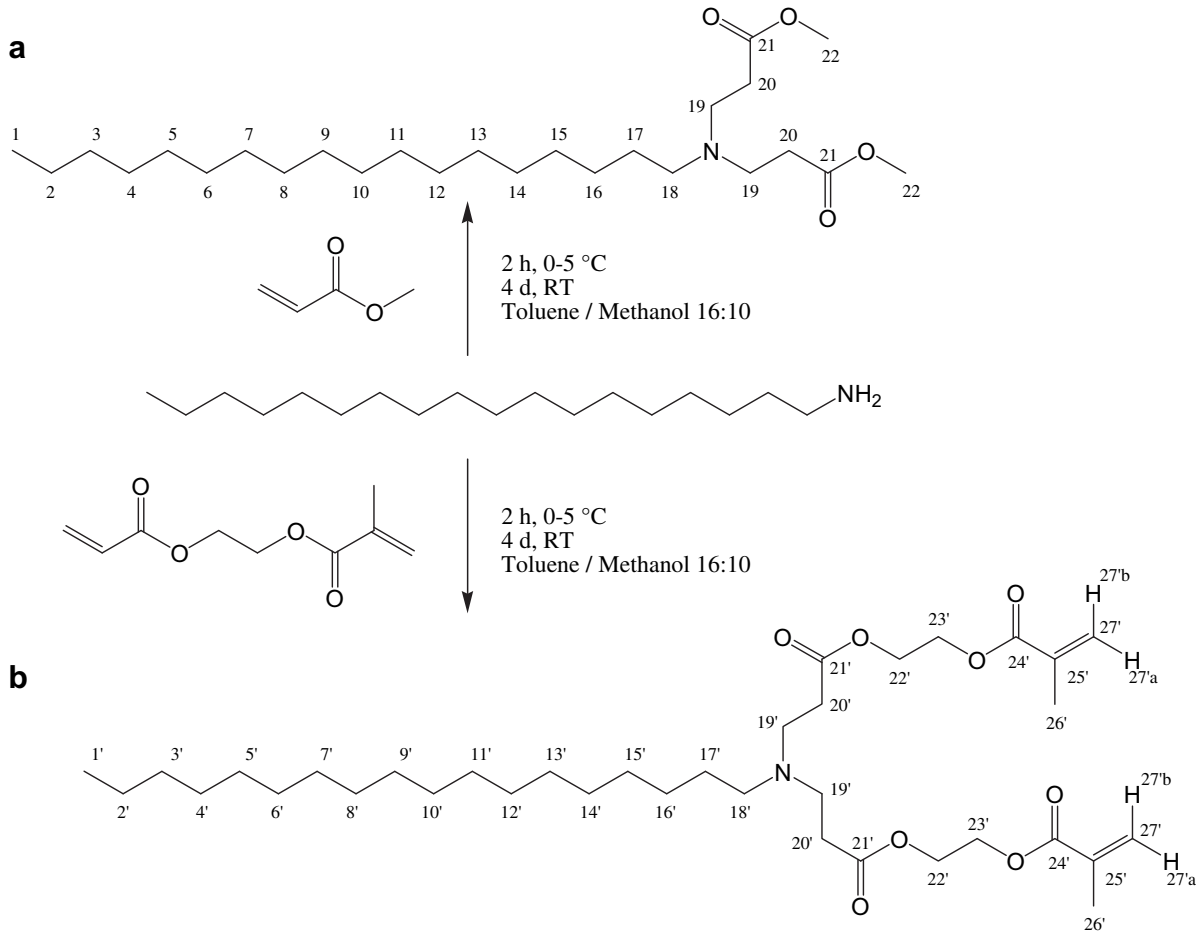

Scheme 2. Michael addition synthesis and structures of tertiary amines. (a) Ester-functional amine SAE; (b)methacrylate-functional amine SAMA.

monomer SR368 were supplied by Sartomer, Germany. Genomer 4302 (G4302) was supplied by Rahn AG, Switzerland. The photoinitiator Irgacure 784 was supplied by Ciba Specialty Chemicals Inc. All chemicals were used as received if not stated otherwise.

2.2. Synthesis of swelling agents

2.2.1. Synthesis of stearyl di(methoxy-carbonylethyl) amine (SAE)

SAE was prepared according to the procedure of Weickmann (Scheme 2a) [26]. Methyl acrylate (29.20 g, 0.340 mol) was dissolved in a toluene/methanol-mixture (150 ml, 16/10). Stearyl amine (45.75 g, 0.170 mol), dissolved in a toluene/methanol-mixture (500 ml, 16/10), was added to the methyl acrylate solution at 0–5 °C under stirring within 3 h. After completion of the addition, the mixture was allowed to react for a further 24 h at room temperature. The solvent was evaporated and the product was dried under vacuum. Yields of up to 93% were obtained.

^{1}H NMR (300 MHz, $CDCl_3$): δ = 3.69 (22), 2.88 (19), 2.60 (20), 2.53 (18), 1.50–1.26 (2–17), 0.88 (1); ^{13}C NMR (75.4 MHz, $CDCl_3$): δ = 174.6 (21), 55.2 (18), 52.9 (22), 51.1 (19), 35.8 (20), 24.0–33.9 (2–17), 15.4 (1).

2.2.2. Synthesis of stearyl di(methacryloxyethyl carboxylethyl) amine (SAMA)

2-Methacryloxyethyl acrylate was prepared according to a synthesis reported by Luchtenberg and Ritter Scheme 2b [27]. In short, acryloyl chloride was slowly added to a solution of 2-hydroxyethyl methacrylate and triethyl amine in toluene at 0–5 °C. After completion of the reaction, precipitated triethyl ammonium chloride was removed by filtration and the solvent was evaporated. The resulting product was isolated by fractional vacuum distillation. Yields of up to 83% were obtained.

SAMA was prepared according to Weickmann et al. [27]. 2-Methacryloxyethyl acrylate (50.40 g, 0.273 mol) was dissolved in a toluene/methanol-mixture (180 ml, 16/10). To the resulting solution, stearyl amine (36.77 g, 0.137 mol), dissolved in a toluene/methanol-mixture (600 ml, 16/10), was added at 0–5 °C under stirring within 2 h. After completion of the addition, the mixture was allowed to react for a further 24 h at room temperature. The solvent was evaporated and the product was dried under vacuum. Yields of up to 94% were obtained.

^{1}H NMR (300 MHz, $CDCl_3$): δ = 6.07 (27′b), 5.53 (27′a), 4.27 (22′, 23′), 2.71 (19′), 2.39 (18′, 20′), 1.89 (26′), 1.20–1.24 (2–17′), 0.82 (1′); ^{13}C NMR (75.4 MHz, $CDCl_3$): δ = 174.0 (21′), 169.2 (24′), 137.8 (25′), 127.7 (27′), 64.2 (23′), 63.8 (22′), 55.6 (18′), 51.0 (19′), 34.0 (20′), 24.5–31.5 (2–17′), 20.1 (26′), 15.9 (1′).

2.3. Resin formulation

The matrix resin was formulated according to a previous publication [17] by stirring a mixture of BHT, CN922, SR368, HDDA and G4302 at ambient temperature until a homogenous solution was obtained. The detailed recipe is summarized in Table 1.

Dispersions of calcium phosphate/layered silicate hybrid nanoparticles were prepared according to the procedure described by Weickmann [26]. The organophilic functionalization agent

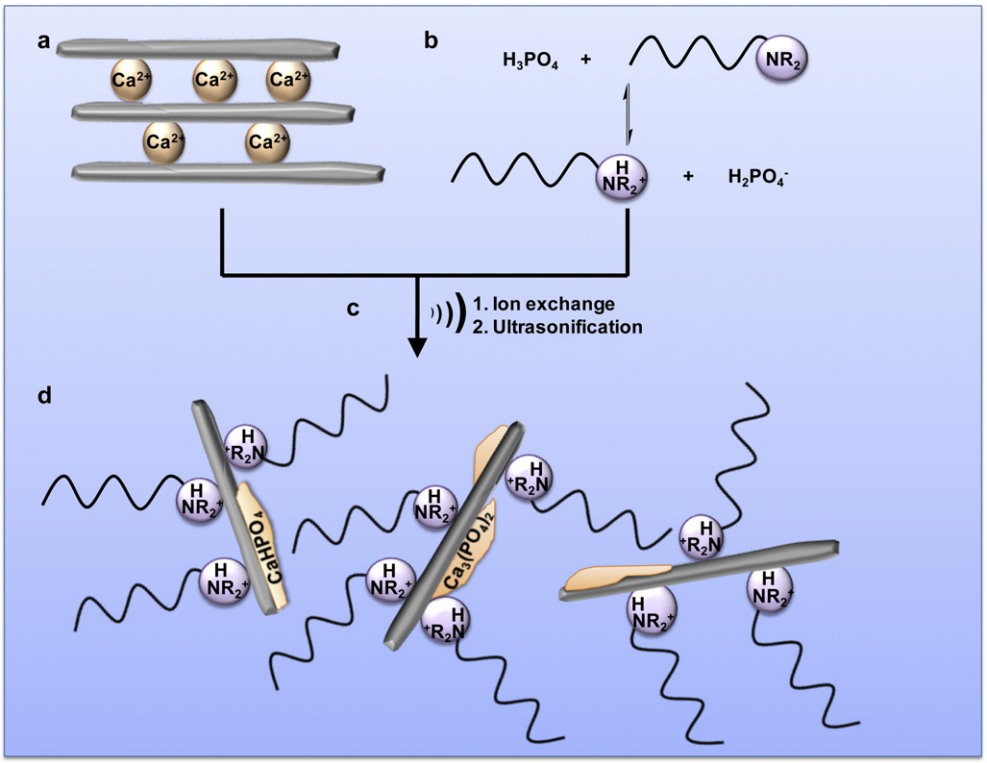

Scheme 3. Preparation of acrylic resins containing in-situ formed calcium phosphate/layered silicate hybrid nanoparticles. (a) Natural Ca-bentonite with intergallery Ca-ions, (b) protonation of organophilic amines by phosphoric acid, (c) exchange of intergallery Ca-ions by quaternary ammonium ions and simultaneous precipitation of calcium phosphate, dispersion by means of ultrasonification and (d) intercalated calcium phosphate/layered silicate hybrid nanocomposites after dispersion and polymerization. All steps of this "one-pot" process are performed in bulk monomer.

(0.8 mmol per g Ca-bentonite) was solved in the matrix resin by stirring for 0.5 h at ambient temperature in a light sealed 500 ml flask. Protonation was carried out by adding phosphoric acid (0.8 mmol per g Ca-bentonite) and stirring for a further 0.5 h. Ca-bentonite was added to the resin and in-situ ion exchange was conducted by stirring the obtained dispersions for 1 h at ambient temperature, followed by ultrasonification (3 × 2 min, max. 60%, Sonoplus HD 2200, Bandelin, Germany). Respective resins were cooled in an ice/water bath during ultrasonification. Samples (ca. 5 g) of each resin were drawn and poured into glass vials to be photographed in regular intervals over 3 months in order to examine sedimentation stabilities. Photoinitiator I784 (1 wt.% with respect to the resin dispersion) was added to the remaining resins and solved by stirring the mixture at ambient temperature for at least 12 h. Resins with varying contents of calcium phosphate/layered silicate hybrid nanoparticles and varying swelling agents were formulated.

2.4. Methods and characterization

2.4.1. SLM apparatus

All SLM processes were performed on a Perfactory Multilens (Envisiontec GmbH) equipped with a mercury vapour lamp that was calibrated to an intensity of 59.0–61.0 W m^{-2} with a standard deviation of less than 0.5 W m^{-2} calculated from intensity-measurements at 13 spots spread uniformly over the whole building envelope (77.90 mm × 62.32 mm). A layer thickness of 50 μm was chosen for all building processes. The layer curing times were adjusted to obtain a uniform curing depth of 80 μm for each respective resin, leading to an overlap of 30 μm between adjacent layers. The obtained specimens were cleaned with 2-propanol. For the design and dimensions of all specimens, see the Supplementary part.

2.4.2. Postcuring

UV-postcuring was executed under a UV-lamp (HPL-R 400, 400 W, 230 V, Philips) in a self built light oven. Samples were deposited on a teflon plate positioned 50 mm beneath the lamp. Materials were cured for 30 or 60 min from each flat side of respective specimens, affording overall curing times of 1 or 2 h.

2.4.3. Determination of photochemical parameters

Glass slides were wetted with the respective resin. Defined areas were cured with different curing times (1–48 s). The glass slides were cleared of remaining resin by rinsing them with 2-propanol. Film thicknesses were measured with a digital calliper with an accuracy of ±10 μm. For each resin, three working curves were measured at different positions of the building envelope following the described routine. For adjustment of the building parameters, measured curing depths were calculated as average values for a given resin and exposure time.

2.4.4. Tensile tests

Tensile test were carried out according to ISO 527-2 with type 1BA specimens and a deformation speed of 20 mm s^{-1} on a Zwick Z-005 tensile test machine. The Young's modulus was detected for all materials before (referred to as green strength) and after UV-postcuring.

2.4.5. Fracture toughness

Fracture toughness parameters (K_{1c}) were determined according to the ESIS testing protocol using a modified Zwick tensile testing machine (Zwick 1340) equipped with a peak voltmeter (ERMA, Type U 568.01-FHI). Compact tension specimens were printed using the SLM apparatus. The notch root was sharpened with a razorblade. Tensile loading (mode 1) was carried out at room

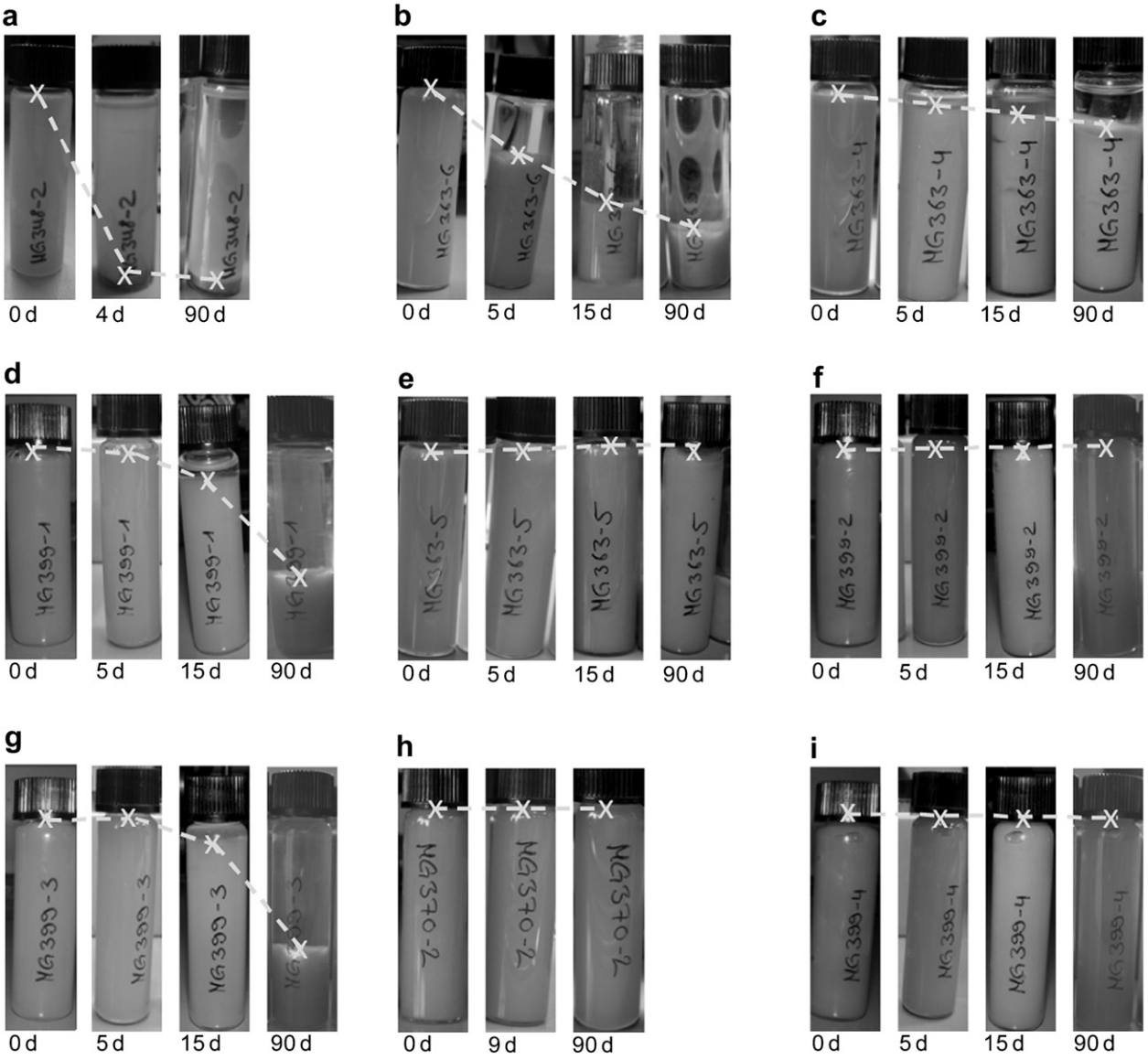

Fig. 1. Sedimentational stability of dispersions containing in-situ formed calcium phosphate/layered silicate hybrid nanoparticles: (a) natural Ca-bentonite dispersed without organophilic functionalization; (b) dispersion of natural Ca-bentonite in-situ functionalized using Ethoquad C12; (c) dispersion of calcium phosphate/layered silicate hybrid nanoparticles containing functionalized using SA; (d–f) dispersions of calcium phosphate/layered silicate hybrid nanoparticles functionalized using SAE; (g–i) dispersions of calcium phosphate/layered silicate hybrid nanoparticles functionalized using SAMA.

temperature with a deformation speed of 2 mm min^{-1}. The fracture surfaces of the CT specimens were investigated using an Environmental Scanning Electron Microscope (ESEM 2020, Electroscan Corp.) and optical microscopy (Leitz Aristomet).

Table 2
Brookfield viscosities (25 °C, 15 s^{-1}) and photochemical parameters for unfilled model resin and calcium phosphate/layered silicate hybrid nanoparticle dispersions.

Resin	η[mPa s][a]	D_p[μm m^2 J^{-1}]	E_c[J m^{-2}]	E_{80}[J m^{-2}]
Pure Resin	249	147	68.4	117.7
SAE-5	340	124	21.0	40.1
SAE-10	1050	129	18.2	33.9
SAE-15	1466	178	26.9	42.3
SAMA-5	307	172	31.5	50.1
SAMA-10	656	203	31.1	46.1
SAMA-15	1236	211	29.4	43.0

[a] Brookfield viscosity, measured at 25.0 °C and 15 s^{-1}.

2.4.6. Transmission electron spectroscopy

Samples for TEM were prepared using a Leica Ultracut UCT at room temperature. Thin slices (ca. 100 nm) of the respective material were investigated with a TEM microscope (LEO CEM 912), using an acceleration voltage of 120 kV.

2.4.7. Polymerization shrinkage-density measurement

Densities of liquid resins were determined at 25 °C using a light sealed pycnometer (10 ml, Schott). Densities of cured materials before and after UV-postcuring were calculated after sinking each respective material in mineral oil (Shell Vitrea 100) at 23 °C following the principle of Archimedes. Volumetric polymerization shrinkages were calculated from measured densities [28].

2.4.8. Distortion analysis-H-shaped diagnostic part

To quantify distortion phenomena occurring at different stages of the building process, 5 H-shaped diagnostic parts were built

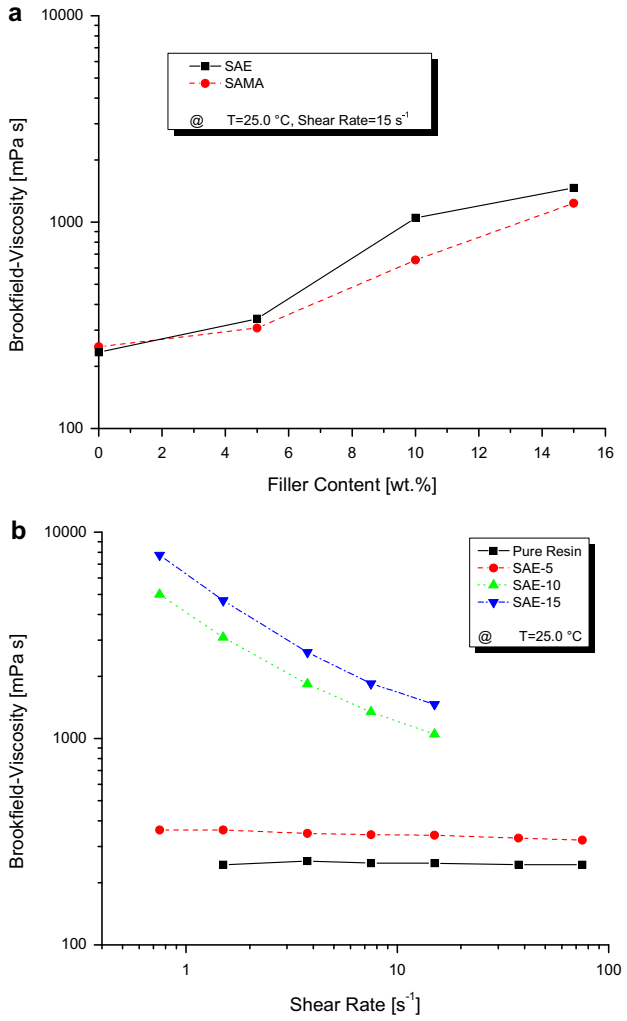

Fig. 2. Brookfield viscosities of calcium phosphate/layered silicate hybrid nanoparticle dispersions; (a) Influence of filler content and swelling agent on resin viscosity and (b) Structural viscosity, shear thinning of dispersions formed by in-situ swelling of Ca-bentonite using SAE as swelling agent.

according to CAD data (width 40.0 mm, height 17.5 mm, bar thickness 2.5 mm, no support structures) for each resin using the SLM process. Stress relaxation due to distortion was prevented by a 1.0 mm thick baseplate connecting the legs of all specimens as parts were stored in the darkness at room temperature for 6–12 h. Parts were measured in the green state 1 h after removal of the baseplate to determine linear green shrinkage and green effective ankle splay out. The specimens were UV-postcured with a delay of

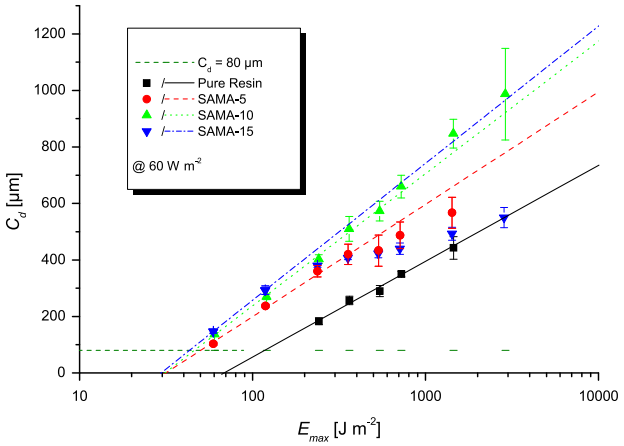

Fig. 3. Working curves of calcium phosphate/layered silicate hybrid nanoparticle dispersions in comparison to pure resin. Dispersions of natural Ca-bentonite rendered organophilic with SAMA.

2 h after removal of the baseplate and measured again 24 h afterwards. All measurements were carried out using an optical microscope (UWM 1, Leitz Wetzlar) equipped with a position measuring system (VRZ 181, Heidenhain). Analysis and interpretation of measured values was performed according to Pang [29]. The ankle position was measured at the interface of the H-shaped specimen and the interconnecting baseplate used to prevent premature distortion. Lateral distortion was not analyzed.

2.4.9. Viscosity

All viscosities were measured using a viscosimeter with cone-plate-geometry (Brookfield RV-DV-II, cone type CPE 40, cone angle 0.8°, 0.1–10.0 rpm, 25.0 ± 0.1 °C, sample volume 0.5 ml).

3. Results and discussion

3.1. Resin formulation

The formulation of the unfilled matrix resin by blending together the acrylate functionalized oligomers Genomer 4302 (G4302) and Sartomer CN922 with the monomer tris(2-hydroxyethyl)isocyanurate triacrylate (SR368), the reactive diluent hexanediol diacrylate (HDDA) and the inhibitor 2,6-di-*tert*-butyl-4-methylphenol (BHT) according to Table 1 was described previously [17]. Dispersions of in-situ formed calcium phosphate/layered silicate hybrid nanoparticles have been prepared via in-situ ion exchange reaction of quaternary ammonium ions for the intergallery Ca^{2+} of Ca-bentonite using solvent-free Ca-bentonite suspensions in the monomer mixture. The ammonium ions used to render the bentonite's silicate layers organophilic were in-situ generated by

Table 3
Mechanical and micromechanical properties of unfilled benchmark and nanocomposite materials. Young's modulus determined in tensile experiments at different stages of the postcuring processes, critical stress intensity factors K_{1c} determined from tensile experiments on pre-notched CT specimen postcured for 1 h. Layer orientations implemented during the building procedure were parallel to tensile load direction.

Resin	Young's modulus green state [MPa]	Young's modulus postcured 1 h [MPa]	Young's modulus postcured 2 h [MPa]	K_{1c} postcured 1 h [MPa m$^{1/2}$]
Pure Resin	500 ± 20	1290 ± 30	1240 ± 60	0.35 ± 0.03
SAE-5	560 ± 80	1320 ± 40	1370 ± 70	0.35 ± 0.02
SAE-10	660 ± 30	1620 ± 30	1630 ± 40	0.39 ± 0.03
SAE-15	720 ± 90	1740 ± 60	1710 ± 50	0.45 ± 0.01
SAMA-5	600 ± 70	1440 ± 30	1480 ± 40	0.36 ± 0.03
SAMA-10	620 ± 30	1407 ± 60	1500 ± 70	0.42 ± 0.05
SAMA-15	670 ± 30	1510 ± 110	1600 ± 50	0.44 ± 0.02

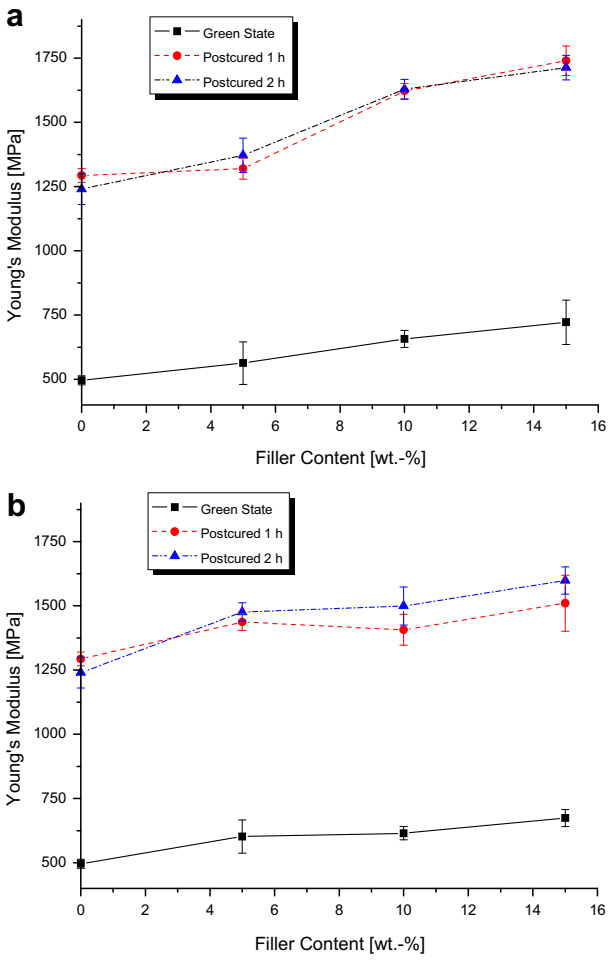

Fig. 4. Photopolymerized and postcured materials stiffness as function of hybrid nanoparticle content. (a) Dispersions formed by in-situ functionalization of natural Ca-bentonite with organophilic ester-functional swelling agent SAE and (b) respective materials obtained using swelling agent SAMA containing reactive methacrylic moieties.

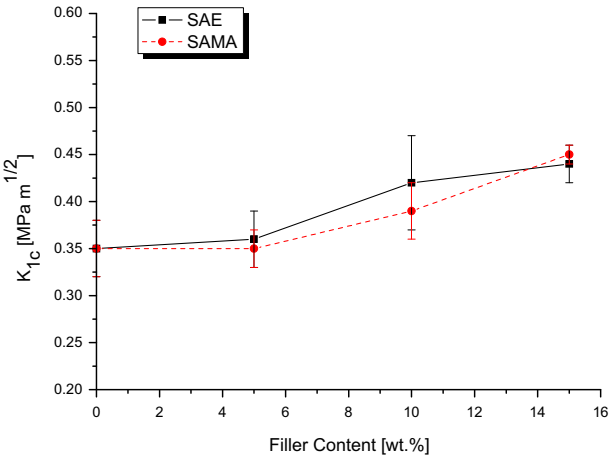

Fig. 5. Fracture toughness expressed as critical stress intensity factor K_{1c} for the postcured unfilled reference material and nanocomposites containing in-situ formed calcium phosphate/layered silicate hybrid nanoparticles rendered organophilic by ion exchange of intergallery Ca^{2+} with protonated SAE or SAMA.

phosphoric acid-mediated protonation of stearyl amine (SA), the ester-functional stearyl di(methoxy-carbonylethyl) amine (SAE), prepared via Michael addition of SA with two methylacrylates, or the methacrylate-functional stearyl di(methacryloxyethyl-carbonylethyl) amine (SAMA), prepared by in-situ Michael addition of SA to the acrylate group of 2-methacryloxyethyl acrylate [27]. The ion exchange was accompanied by the simultaneous precipitation of calcium phosphate at the interfaces of the silicate layers, thus forming hybrid particles. The resulting dispersions (SA/SAE/SAMA-*x* with *x* representing the filler content in wt.%) were photopolymerized without any further purification. Additional steps like washing, drying, milling and dispersion typical for conventional organoclay preparation in aqueous medium were not necessary following the described one-step procedure that was introduced by Weickmann et al. [26]. The preparation of acrylic dispersions is illustrated in Scheme 3.

3.2. Resin properties

Resins suitable for SLA and SLM processing have to fulfil several requirements that are of minor importance for conventional thermosets [7]. Application in photochemical RP requires the resins properties to remain constant under processing conditions for days up to several weeks, as part of the resin remains in the vat after completion of each building process. Consecutively, resins containing dispersed filler particles should not exhibit sedimentation within this time frame. The sedimentation stability of resins containing calcium phosphate/layered silicate hybrid nanoparticles was therefore investigated over a period of 90 days (Fig. 1). Photographic images illustrating dispersion stabilities as a function of the filler contents for different organophilic functionalization agents can be found in the supporting information.

Comparison of resins with filler contents of 5 wt.% leads to the conclusion that dispersions containing hybrid nanoparticles are more stable than dispersions of both natural Ca-bentonite and organoclay obtained by in-situ swelling with a commercial quaternary exchange agent (Ethoquad C12, Akzo-Nobel). However, even using the most efficient organophilic amines SAE or SAMA, filler contents of 10 wt.% or higher are needed to obtain dispersions that show no visible sedimentation within the range of three months. These amines were therefore chosen for the preparation of resins for SLM processing. Samples with 5 wt.% calcium phosphate/layered silicate hybrid particles remain homogenous over days, but show moderate settlement within the range of weeks. Lower filled resins were stirred after each building procedure to prevent filler sedimentation.

Maximum filler contents for successful SLM processing were determined by measuring Brookfield viscosities of the unfilled reference resin and calcium phosphate/layered silicate hybrid particle dispersions (Table 2).

Respective viscosities increase significantly from 249 mPa s for the pure acrylic resin up to 1269 mPa s for SAE-15 and 851 mPa s for SAMA-15 (Fig. 2a). The comparably lower viscosities observed for layered silicate dispersions swollen with SAMA may be explained by the lower inorganic content at a given overall hybrid particle content. All hybrid nanoparticle dispersions show distinct shear thinning, thus reflecting the presence of anisotropically shaped filler particles. The shear rate dependence increases significantly with the organoclay content (Fig. 2b). In the case of SAE-15, the range of observed Brookfield viscosities varies from 1466 mPa s at a shear rate of 15 s^{-1} to 7750 at 0.75 s^{-1}. The strong increase of the viscosity and the influence of the shear rate from dispersions containing 5 wt.% to those containing 10 wt.% filler correlates with the enhanced sedimentation stability observed for the highly filled resins. It may be attributed to a structural change from isolated hybrid particles to a network of percolating particle

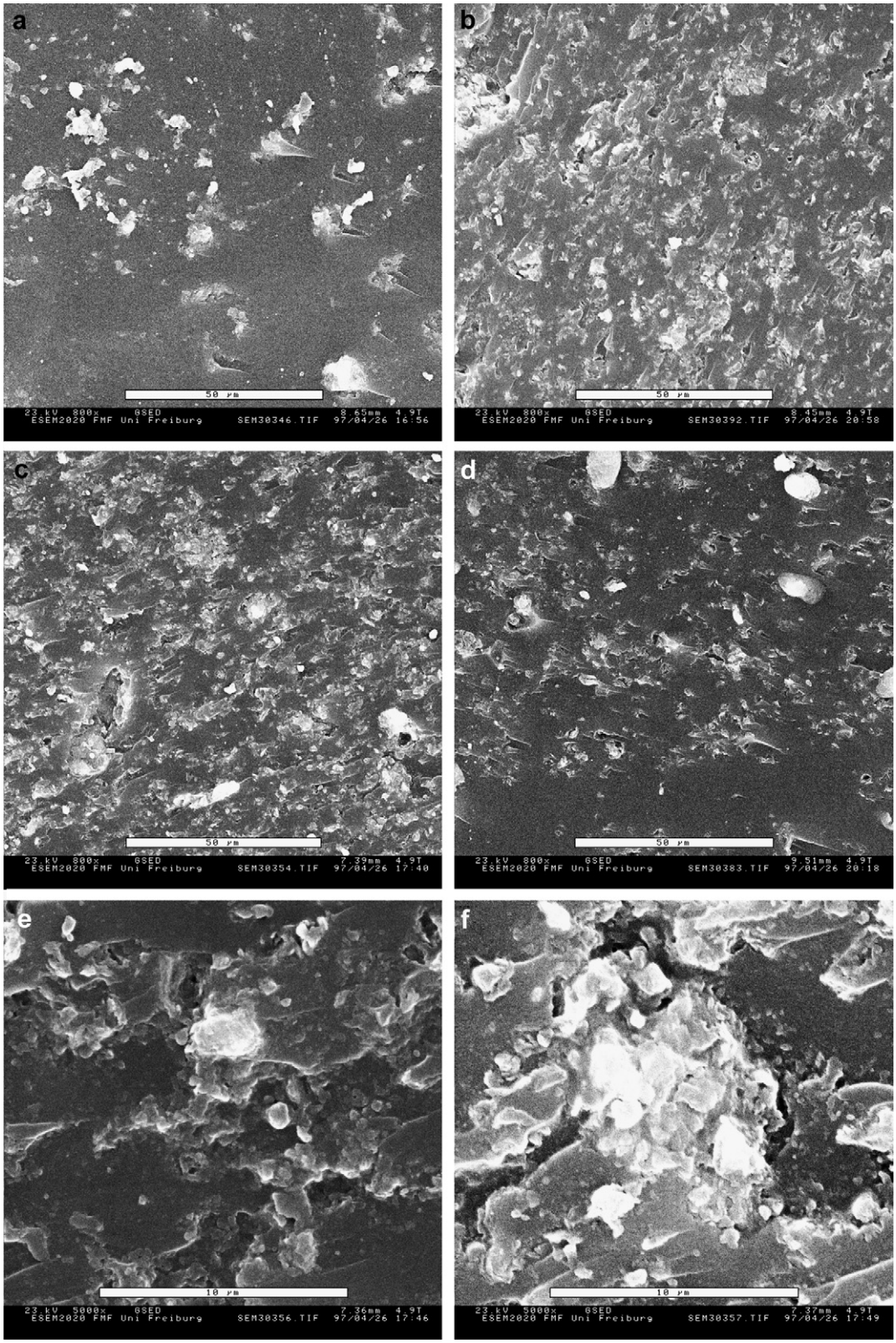

Fig. 6. Fracture mechanics analysis. Characterization of fracture surfaces derived from fractured CT specimens by means of environmental scanning electron microscopy. Increasing surface roughness with increasing filler content illustrated at the example (a) SAE-5, (b) SAE-10, (c,e–f) SAE-15 and (d) SAMA-15. Crack tip propagation from left to right in all cases.

fragments. In addition, it was found that dispersions with organoclay contents above 15 wt.% were not processable via SLM. Yet, the distinct shear thinning observed at elevated filler contents may allow for successful processing of the paste-like dispersions using techniques that employ higher shear rates to distribute resins. Resins with filler contents up to 15 wt.% were successfully processed via SLM with uniform layer-waiting times of 1.0 s (at levelling) and 0.5 s (at peeling).

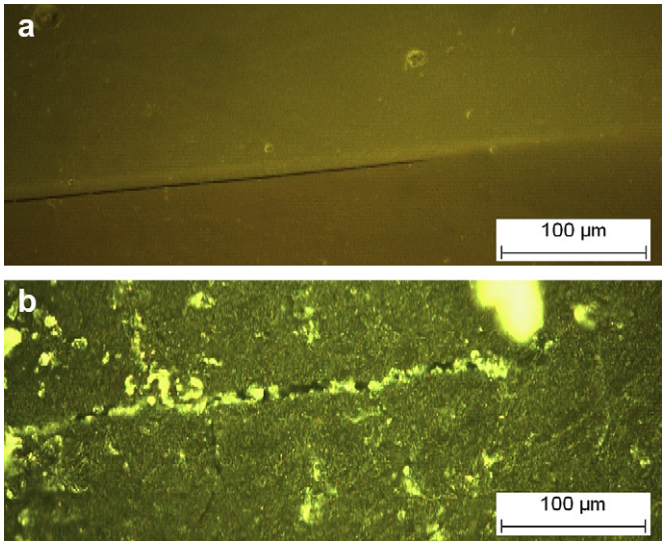

Fig. 7. Morphology of crack tip damage zones, observed using optical microscopy. (a) Unfilled benchmark material and (b) SAE-10. Crack propagation from left to right in all cases.

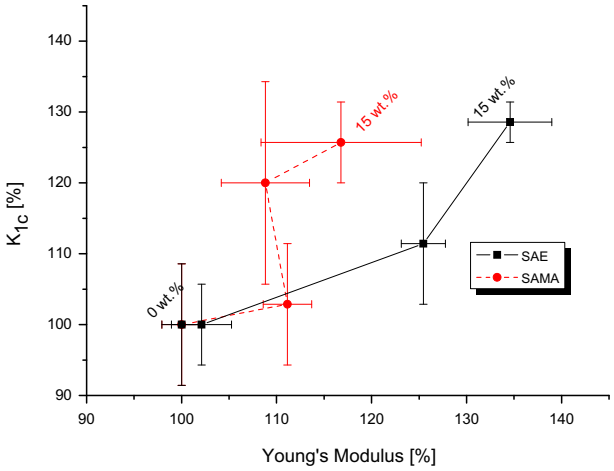

Fig. 8. Improved stiffness/toughness balance of nanocomposites containing in-situ formed calcium phosphate/layered silicate hybrid nanoparticle dispersion. All materials were postcured for 1 h and loaded parallel to the layer orientation implemented in SLM processing.

Photochemical parameters of the pure acrylic resin and dispersions containing in-situ formed hybrid nanoparticles were determined by relating the curing depth (C_d) to the maximum curing exposure (E_{max}) calculated from the curing time (C_t) and the curing energy density (60.0 W m^{-2}, measured at the bottom SLM apparatus' vat). The correlation commonly referred to as working curve can be described theoretically using Equation (1) [2]. The photochemical behaviour of all developed resins fulfils equation (1) in the exposure range relevant for SLM processing with a layer thickness of 50 µm (Fig. 3 and Table 2). All hybrid particle dispersions show enhanced photosensitivity in comparison to the unfilled acrylic resin, as expressed by a significant decrease of the critical

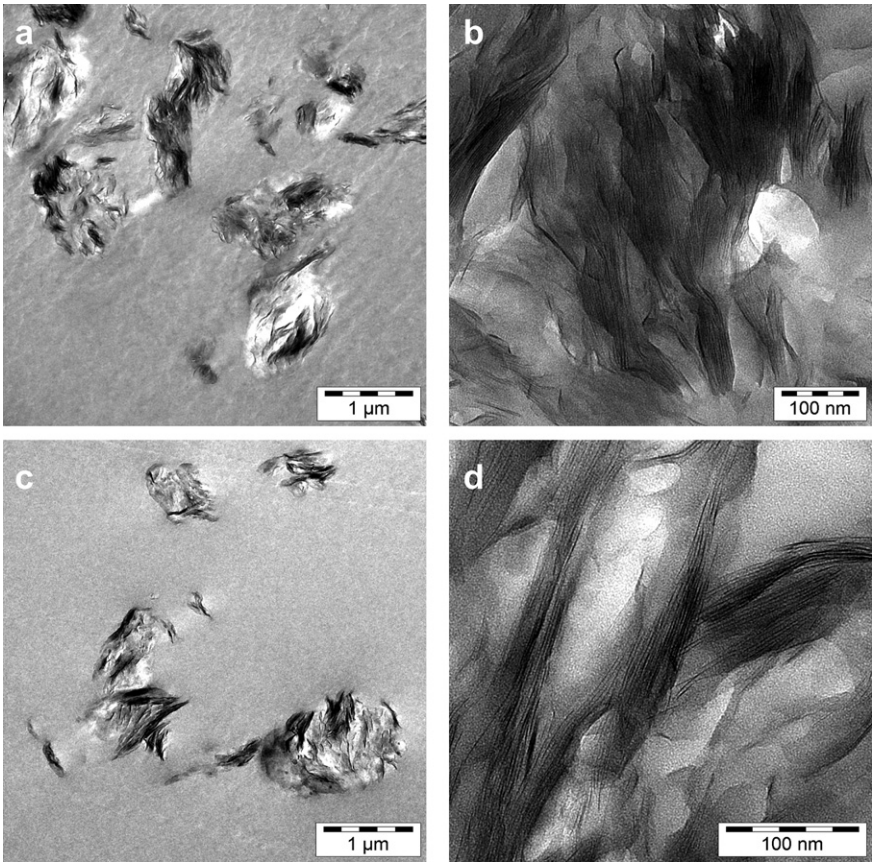

Fig. 9. Nanocomposite morphologies characterized using TEM. (a) Dispersion of particles in SAE-10 showing loosely agglomerated silicate layer packages with average diameters in the range of 1 µm; (b) high magnification TEM reveals intercalated and exfoliated layers. (c–d) Morphologies obtained for SAMA-10.

energy necessary for network formation (E_c) from 68.4 J m^{-2} for the pure resin to an exposure between 20 J m^{-2} and 30 J m^{-2} for all nanocomposite resins. The corresponding penetration depths (D_p) are less affected by the calcium phosphate/layered silicate particle content, showing only slight increases from 147 μm m^2 J^{-1} for the pure resin to 178 μm m^2 J^{-1} for SAE-15 and 211 μm m^2 J^{-1} for SAMA-15, respectively. The increased photosensitivity may be explained by multiple reflection of photons by dispersed filler particles, leading to higher quantum yields. An exposure sufficient for a C_d of 80 μm (C_{80}) was chosen to guarantee sufficient overlap of adjacent 50 μm layers in SLM processing. C_{80} is lowered from 117.7 J m^{-2} for the benchmark resin to a value between 33.9 J m^{-2} and 50.1 J m^{-2} for calcium phosphate/layered silicate hybrid particle dispersions. The corresponding layerwise C_t decreases from 2.0 s for the unfilled resin to values between 0.7 s and 1.0 s for resins containing organoclay.

$$C_d = D_p[\ln(E_{max}) - \ln(E_c)] = 2.303 D_p[\log(E_{max}) - \log(E_c)] \quad (1)$$

Specimens for the characterization of key material properties were successfully plotted according to CAD data from the unfilled reference resins and dispersions of Ca-bentonite functionalized using SAE and SAMA. Material properties were determined before (referred to as green state) and after postcuring. Postcuring was carried out in a UV light oven either for 1 h or for 2 h.

3.3. Mechanical and micromechanical properties

The stiffness of the photopolymerized pure resin and calcium phosphate/layered silicate hybrid nanoparticle dispersions containing either SAE or SAMA was characterized determining each material's respective Young's Modulus (Table 3) in tensile experiments with dog bone specimens that were 3D plotted using the SLM process. Nanocomposite materials show significantly increased stiffness with increasing filler contents both in the green and postcured state (Fig. 4). The strengthening effect is more effective for particles rendered organophilic with SAE than for those treated with SAMA, obtaining a green strength of 720 MPa for SAE-15 and 620 MPa for SAMA-15 in comparison to 500 MPa for the unfilled resin. The stiffness of respective materials after UV-postcuring for 1 h is significantly higher and increase in parallel with increasing filler content, from 1290 MPa for the pure resin up to 1740 MPa for SAE-15 and 1510 MPa for SAMA-15. Extended

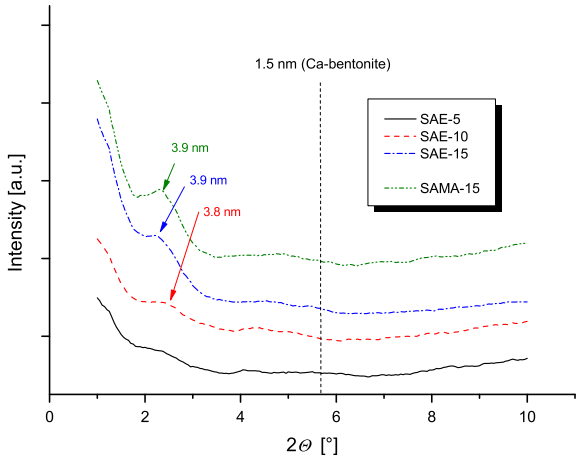

Fig. 10. WAXS diffraction patterns of nanocomposites containing in-situ formed calcium phosphate/layered silicate hybrid particles. Materials show reflexes in the range of $2\Theta = 2–3°$, corresponding to intergallery spacings of 3.8–4.0 nm.

postcuring does not enhance stiffness any further, thereby indicating that crosslinking is completed after 1 h of postcuring.

While the strengthening of resins for SLM and SLA has been reported before, toughness, which may be the more crucial property for these materials has not been investigated. The toughness of materials obtained from SLM processing of acrylic in-situ formed calcium phosphate/layered silicate hybrid nanoparticle dispersions were determined as critical stress intensity factors K_{1c} from the maximum load applied in tensile tests conducted with pre-notched compact tension specimens (Table 3). Nanocomposite materials show a significant increase in fracture toughness with increasing filler content. At a filler content of 15 wt.%, a K_{1c} of 0.45 MPa m$^{1/2}$ for SAE-15 and 0.44 MPa m$^{1/2}$ for SAMA-15 is obtained. Compared to the critical stress intensity parameter of 0.35 MPa m$^{1/2}$ for the unfilled benchmark resin, incorporation of hybrid particles accounts for a relative increase of 29% in the case of postcured SAE-15 (Fig. 5).

Fracture mechanics analysis of fracture surfaces derived from tensile experiments by means of environmental scanning electron microscopy strengthens the reported toughness increase. With increasing content of calcium phosphate/layered silicate hybrid

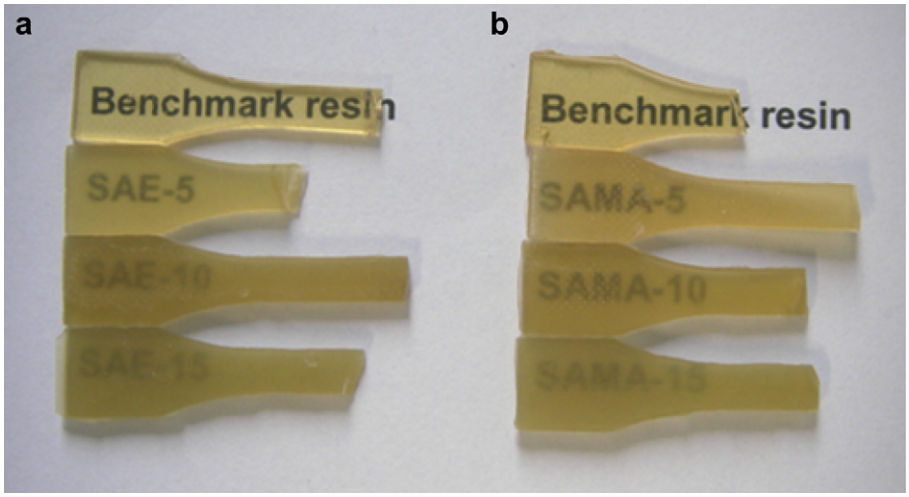

Fig. 11. Optical appearance of nanocomposites containing in-situ formed calcium phosphate/layered silicate hybrid nanoparticles. Increasing turbidity with increasing filler content of dispersions containing Ca-bentonite functionalized with (a) SAE and (b) SAMA.

Table 4
Volumetric polymerization shrinkages and distortions measured on SLM processed H-shaped diagnostic parts of unfilled benchmark and nanocomposite materials before and after postcuring.

Resin	Vol. Polym. Shrink. Green [%]	Vol. Polym. Shrink. Postcured [%][a]	Lin. Green Shrink. [%]	Lin. Postcuring Shrink.[%][a]	Eff. Ankle Splay Out Green [mm]	Effective Ankle Splay Out Postcured [mm][a]
Pure Resin	9.7 ± 0.4	12.2 ± 0.4	1.04 ± 0.37	0.51 ± 0.29	1.38 ± 0.13	1.73 ± 0.06
SAE-5	10.2 ± 1.6	11.9 ± 0.3	1.48 ± 0.06	0.54 ± 0.06	1.02 ± 0.08	1.38 ± 0.23
SAE-10	9.8 ± 0.7	11.3 ± 1.4	1.08 ± 0.06	0.51 ± 0.10	1.06 ± 0.08	1.18 ± 0.08
SAE-15	8.9 ± 0.2	9.4 ± 1.8	0.71 ± 0.18	0.45 ± 0.09	1.04 ± 0.19	1.18 ± 0.18
SAMA-5	10.7 ± 0.5	11.6 ± 0.3	0.96 ± 0.07	0.65 ± 0.06	1.23 ± 0.07	1.63 ± 0.12
SAMA-10	7.8 ± 1.2	10.0 ± 0.3	0.97 ± 0.26	0.53 ± 0.15	1.19 ± 0.12	1.32 ± 0.04
SAMA-15	8.6 ± 0.5	9.5 ± 0.3	0.93 ± 0.17	0.57 ± 0.07	1.22 ± 0.05	1.48 ± 0.06

[a] UV-postcured for 1 h.

particles, an increased surface roughness is observed (Fig. 6a–d). The roughness reflects a more indirect crack propagation through nanocomposite materials, accounting for additional energy dissipation as the hybrid particle agglomerates are circumvented. As the crack tip propagates through the heterogeneous material, crack opening requires pulling out of the compact agglomerates, consuming additional energy. Higher magnification ESEM micrographs show both bare micron-sized agglomerates that were excavated from the matrix and the corresponding cavities (Fig. 6e–f). Optical microscopy carried out on the crack tip damage zone in the unfilled benchmark material and nanocomposites strengthens the proposed mechanism of failure. Fig. 7 illustrates how crack propagation through the nanocomposite material is altered by the hybrid particle agglomerates deflecting the crack tip. Excavated filler particle agglomerates become visible as bright traces all along the crack opening.

Analyzing fracture surfaces, no layered microstructures can be observed, thereby indicating that the postcured materials exhibit isotropic mechanical properties regardless of their organoclay content.

The overall improved stiffness/toughness balance achieved upon incorporation of in-situ formed hybrid nanoparticles is summarized in Fig. 8. Best results were obtained with dispersions based on Ca-bentonite that was in-situ functionalized by ion exchange with SAE, exhibiting stiffness and toughness improved by 35% and 30% with respect to the unfilled material at 15 wt.% filler content.

3.4. Morphology and optical properties

The morphology of the developed nanocomposite materials was characterized by means of Atomic Force Microscopy (AFM), TEM and WAXS. Using AFM, it was shown for the unfilled reference material that no phase separation occurs within the polymeric matrix [17]. Nanocomposites containing Ca-bentonite subjected to an in-situ ion exchange of the intergallery Ca^{2+} for organophilic quaternary ammonium ions show well dispersed calcium phosphate/layered silicate hybrid particles (Fig. 9). The primary particles with diameters above 10 μms are fragmented during the one-step swelling procedure and subsequent photopolymerization into particles with average diameters in the range of 1 μm (Fig. 9b,c). Within these particles, silicate layers are organized in a rather loose fashion. High magnification TEM reveals the presence of both intercalated and exfoliated layers (Fig. 9c).

WAXS diffraction patterns of the postcured nanocomposite materials do not show peaks at $2\Theta = 5.9^{\circ}$, corresponding to the basal spacing of 1.5 nm observed for natural Ca-bentonite. It can be concluded that all silicate layers have been widened by in-situ ion exchange and subsequent polymerization, leading to complete intercalation and allowing for partial exfoliation. Intercalated layers show intergallery spacings between 3.8 and 4.0 nm ($2\Theta = 2.0–3.0^{\circ}$), whereas the filler content and the type of swelling agent used in organophilic functionalization appear to be of minor influence (Fig. 10). Enhanced intercalation and exfoliation reported for other nanocomposites based on organoclays featuring surface functionalization agents equipped with reactive groups could not be observed for nanocomposites containing SAMA. Obviously, the rather high molecular weight oligomers in the matrix resin formulation lack the mobility necessary for diffusion between the silicate layers in the hybrid nanoparticles, thereby preventing effective intergallery polymerization.

The optical appearance of a nanocomposite is generally strongly dependent on the type and amount of filler and on the composite morphology. The polymeric matrix used in this study has been shown to be transparent even at high filler concentrations in nanocomposites containing uniformly dispersed spherical silica particles with diameters small enough not to implement significant light scattering [17]. Nanocomposites of bentonites cannot be expected to exhibit transparent optical appearance, but to be translucent in the best case. The materials derived from photopolymerization of calcium phosphate/layered silicate hybrid nanoparticle dispersions reflect this general behaviour by showing increasing turbidity with increasing filler content (Fig. 11). An influence of the type of swelling agent used for organophilic functionalization cannot be observed when comparing samples with identical filler content.

3.5. Polymerization shrinkage, internal stresses and distortion phenomena

Many of the growing number of applications for photochemical RP technologies require the respective processes to be carried out

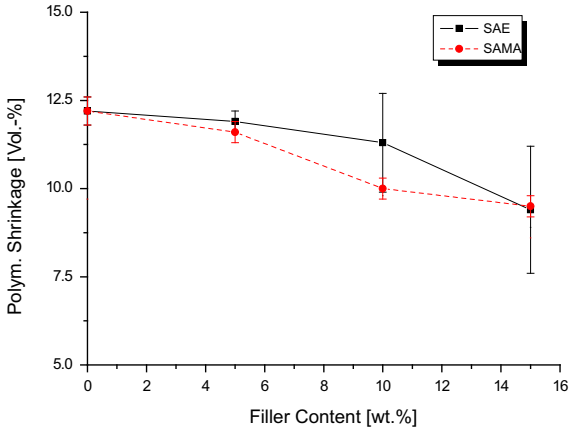

Fig. 12. Volumetric polymerization shrinkages of postcured materials with varying filler contents and organophilic functionalization agents. Shrinkages are deduced from density measurements conducted in mineral oil at 25.0 °C.

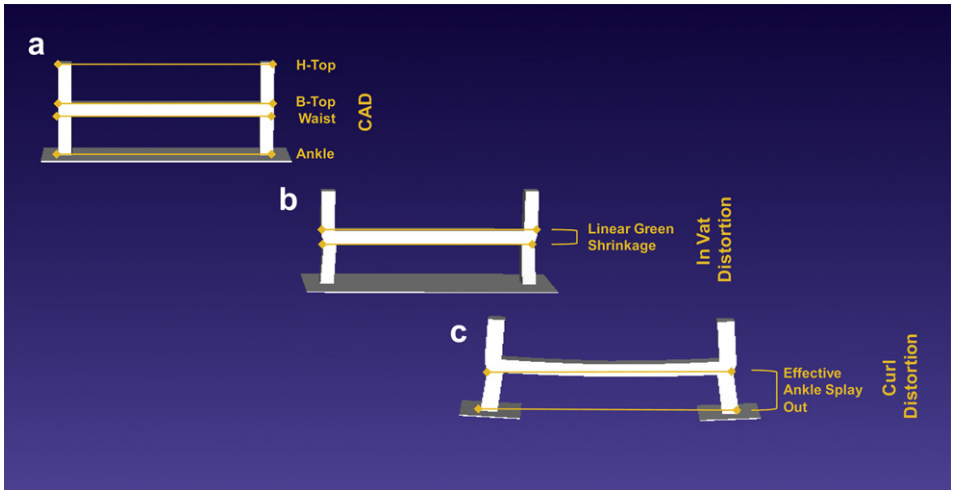

Scheme 4. Analysis of distortion phenomena by means of processing and characterization of H-shaped diagnostic parts. (a) CAD data of H-shaped diagnostic part with critical dimensions and interconnecting polymer film that ensures adhesion to the building platform and prevents premature ankle splay out; (b) SLM processed after removal of the platform, showing linear green shrinkage; (c) diagnostic part after removal of interconnecting polymer film, exhibiting ankle splay out.

with high accuracy. In order to quantify building accuracy, volumetric polymerization shrinkages exhibited by the unfilled benchmark resin and calcium phosphate/layered silicate hybrid nanoparticle dispersions have been deduced from density measurements following the principle of Archimedes [28]. Results are included in Table 4 and plotted as a function of the filler content in Fig. 12. The volumetric polymerization shrinkage decreases with increasing content of calcium phosphate/layered silicate hybrid particles, the latter being inert with respect to the free radical polymerization. The decrease can be observed most significantly for the postcured materials, exhibiting polymerization shrinkages of 12.2% for the unfilled sample in comparison to 9.4% for SAE-15 and 9.5% for SAMA-15, respectively. Shrinkage occurring during photopolymerization of resins for SLM and SLA does not only cause dimensional deviations from CAD data, but may also lead to the development of internal stresses when shrinking layers interact with their ready-built, adjacent counterparts. Curl distortions occur when stresses relax, leading inaccuracies that cannot be met with dimensional compensation factors [2,29].

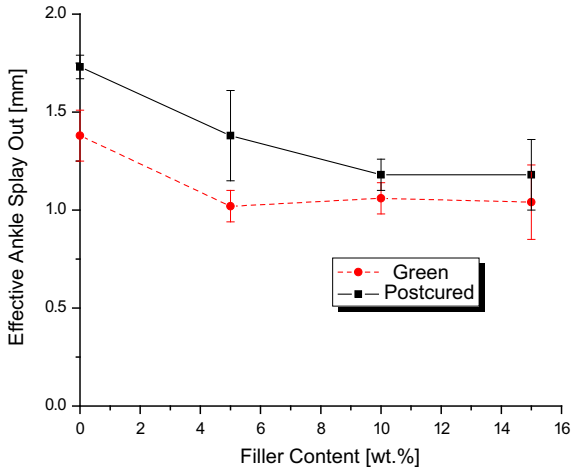

Fig. 13. Green and postcured effective ankle splay out determined from SLM processed H-shaped diagnostic parts for dispersions of calcium phosphate/layered silicate hybrid nanoparticles with organophilic functionalization based on SAE.

While different approaches have been reported to characterize curling induced by internal stresses, plotting and characterization of H-shaped diagnostic parts has been applied frequently due to its versatile output [29]. During SLM or SLA processing of the H-shaped CAD-file, the real part undergoes different distortion phenomena, beginning with the formation of a waist when curing the first layers of the lateral part (linear green shrinkage) to the splay out of the diagnostic parts' ankles upon removal of the building platform or an interconnecting polymer film (effective ankle splay out green). Further deformation can be quantified after UV-postcuring, when further polymerization shrinkage can be measured by comparison of the dimensions of the upper lateral part (B-top) before and after postcuring (linear postcuring shrinkage) and determining the enhanced ankle splay out in the postcured state (Scheme 4).

Distortions determined using H-shaped diagnostic parts are summarized in Table 4. In the case of linear green shrinkage, no influence of the calcium phosphate/layered silicate particles can be observed, indicating that the diagnostic routine developed for the free surface SLA may not be completely transferable to constrained surface SLM. Moreover, the filler amount does not influence the resin's linear postcuring shrinkage with respect to the experimental error.

More significant results were obtained from the ankle splay out before and after postcuring. Increasing stiffness and decreasing volumetric shrinkage obtained upon addition of hybrid nanoparticles synergistically lead to an improved building accuracy due to reduced curl distortion. The improvement is more effective for dispersions of Ca-bentonite in-situ functionalized using SAE, decreasing effective ankle splay out from 1.38 mm before and 1.73 mm after postcuring for the unfilled benchmark resin to 1.05 mm (−30%) and 1.18 mm (−46%) for SAE-15 (Fig. 13). Upon addition of 15 wt.% hybrid particles containing SAMA, ankle splay out was determined to be 1.22 mm before and 1.48 mm after UV-postcuring.

4. Conclusions

Dispersion of calcium phosphate/layered silicate hybrid nanoparticles can be considered an efficient approach to improve property profiles of resins suitable for RP processes based on photopolymerization, such as stereolithography and the SLM process.

During in-situ preparation of hybrid nanoparticles conducted directly within the acrylic benchmark resin acting as reactive solvent, Ca-bentonite is quantitatively intercalated or exfoliated by organophilic alkyl ammonium ions to yield dispersions of loosely arranged hybrid nanoparticle agglomerates with mean diameters in the range of a micrometer. At filler contents between 10 and 15 wt.%, the developed dispersions are sedimentation stable for several months. Exhibiting slightly increased viscosities and photosensitivities in comparison to the unfilled benchmark, the photocurable nanocomposites can efficiently be applied to SLM and SLA manufacturing. Cured nanocomposite materials show an overall improvement of key properties of RP materials with increasing filler content. In comparison to the unfilled benchmark system, tensile tests reveal an increase of materials' stiffness by up to 35% in the postcured and 45% in the green state. Corresponding fracture toughness is significantly improved by up to 29%. Toughening of the nanocomposites is related to the dissipation of additional energy caused by crack tip deflection and excavation of agglomerated hybrid nanoparticles. In conjunction with the significant decrease of volumetric polymerization shrinkage resulting from the addition of hybrid nanoparticles, the superior stiffness of nanocomposites leads to an improvement of the accuracy of CAD data reproduction in 3D objects during the layerwise building procedure. Representative diagnostic parts show a decrease of shrinkage and distortion phenomena by up to 46% in comparison to the unfilled benchmark resin.

The simultaneous improvement of stiffness, toughness and building accuracy reported in this work represents an important step toward application of these technologies in Functional Prototyping and Rapid Manufacturing.

Acknowledgement

The authors thank the Deutsche Forschungsgemeinschaft (DFG) for financial support within SFB 428.

Appendix. Supplementary data

Supplementary data associated with this article can be found in the on-line version, at doi:10.1016/j.polymer.2010.08.026.

References

[1] Gebhardt A. New demands–new processes. In: Gebhardt A, editor. Rapid prototyping. Munich: Carl Hanser Verlag; 2003. pp. 1–9.
[2] Jacobs PF, editor. Stereolithography and other RP&M technologies. Dearborn: SME Publications; 1996.
[3] Hull C: UVP Inc. US 4575330 1986.
[4] Pham DT, Gault RS. Int J Mach Tools Manufact 1998;38:1257–87.
[5] Noorani R. Liquid based RP systems. In: Noorani R, editor. Rapid prototyping–principles and application. Hoboken: Wiley; 2006. pp. 57–79.
[6] Johnson DL. Radtech Rep; 2000:11–4.
[7] Hagiwara T. Macromol Symp 2001;175:397–402.
[8] Jacobs PF, editor. Fundamentals of stereolithography. Dearborn: SME Publications; 1992.
[9] Koplin C, Gurr M, Mülhaupt R, Jaeger R. Proc of the Euro-uRapid 2008: p. 315–318.
[10] Ogale AA, Renault T, Dooley RL, Bagchi A, Jara-Almonte CC. SAMPE Quarterly 1991;22:19–25.
[11] Karalekas DE, Antoniou K. J Mater Proc Technol 2004;153–154:526–30.
[12] Zak G, Sela MN, Park CB, Benhabib B. SFF Proc. 1997; p. 17–24.
[13] Sandoval JH, Ochoa L, Hernandez A, Lozoya O, Soto KF, Murr LE, Wicker RB. SFF Proc. 2005; p. 513–524.
[14] Sandoval JH, Soto KF, Murr LE, Wicker RB. J Mater Sci 2007;42:156–65.
[15] Nguyen MT, Nazarov V: American Dye Source Inc. US 6664024 2003.
[16] Taft D, Ogale AA, Paul F, Hunt E, Ahzi S. SFF Proc. 1997; p. 341–348.
[17] Gurr M, Hofmann D, Ehm M, Thomann Y, Kübler R, Mülhaupt R. Adv Funct Mater 2008;18:2390–7.
[18] Steinmann B, Steinmann A: 3D Systems Inc. EP 1508834 2005.
[19] You X, Xu J: DSM. WO 2005045525 2005.
[20] McAloon KT: Zeneca Ltd., US 6001298 1999.
[21] LeBaron PC, Wang Z, Pinnavaia TJ. Appl Clay Sci 1999;15:11–29.
[22] Okada A, Usuki A. Macromol Mater Eng 2006;291:1449–76.
[23] Boo WJ, Liu J, Sue H. J Mater Sci Technol 2006;22:829–34.
[24] Liu T, Tjiu WC, Tong Y, He C, Goh SS, Chung TS. J Appl Polym Sci 2004;94:1236–44.
[25] Suarez DL, Frenkel H. Soil Sci Soc Am J 1981;45:716–21.
[26] Weickmann H, Gurr M, Meincke O, Thomann R, Mülhaupt R. Adv Funct Mater 2010;20:1778–86.
[27] Luchtenberg J, Ritter H. Macromol Rapid Commun 1994;15:81–6.
[28] J. Stansbury, Ge J. Radtech Report 2003; p. 56–62.
[29] Pang TH, Guertin MD, Nguyen HD. SFF Proc. 1995; p. 170–180.